Available online at www.sciencedirect.com
ScienceDirect
Acta Biomaterialia 4 (2008) 1996–2007
Acta BIOMATERIALIA
www.elsevier.com/locate/actabiomat

Shape-memory NiTi foams produced by replication of NaCl space-holders

A. Bansiddhi *, D.C. Dunand

Department of Materials Science and Engineering, Northwestern University, Cook Hall 2220 Campus Drive Evanston, IL 60208, USA

Received 12 February 2008; received in revised form 6 May 2008; accepted 13 June 2008
Available online 27 June 2008

Abstract

NiTi foams were created with a structure (32–36% open pores 70–400 μm in size) and mechanical properties (4–25 GPa stiffness, >1000 MPa compressive strength, >42% compressive ductility, and shape-memory strains up to 4%) useful for bone implant applications. A mixture of NiTi and NaCl powders was hot-isostatically pressed at 950 and 1065 °C and the NaCl phase was then dissolved in water. The resulting NiTi foams show interconnected pores that replicate the shape and size of the NaCl powders, indicating that NiTi powders densified significantly before NaCl melted at 801 °C. Densifying NiTi or other metal powders above the melting point of the space-holder permits the use of NaCl, with the following advantages compared with higher-melting, solid space-holders such as oxides and fluorides used to date: (i) no temperature limit for densification; (ii) lower cost; (iii) greater flexibility in powder (and thus pore) shape; (iv) faster dissolution; (v) reduced metal corrosion during dissolution; (vi) lower toxicity if space-holder residues remain in the foam.
© 2008 Acta Materialia Inc. Published by Elsevier Ltd. All rights reserved.

Keywords: Nitinol; Porous; Bone replacement; Sodium chloride; Hot isostatic pressing

1. Introduction

Porous metallic biomaterials (e.g., stainless steel, chromium–cobalt, titanium and nickel–titanium (NiTi)) represent superior alternatives to traditional non-porous metallic implants for two main reasons. First, open porosity can enhance bone ingrowth and thus improve fixation at the interface between bone and implant. Second, porosity decreases the mismatch in stiffness between bone and implant, thus reducing stress-shielding effects which shorten the lifetime of the implant through bone resorption and loosening [1]. In this regard, porous NiTi is very promising because it has the lowest Young's modulus (61–69 GPa [2]) among the above metallic implant materials. The effective stiffness of porous NiTi may further be reduced by the superelastic effect, which produces near-linear, recoverable strains by a reversible phase transformation, while maintaining a high strength. Indeed, porous NiTi with 30–80% porosity shows average stiffness values as low as that of cortical bone (12–17 GPa) or even cancellous bone (<3 GPa) [3]). Moreover, the superelastic effect (and the related shape-memory effect) can be used to deploy a NiTi foam in the implant location (similarly to deployable stents and staple [4]). Finally, the superelastic strain developed in the implant as a result of normal physiological stresses in the patient may stimulate continuous osteo-conduction useful for long-term fixation.

For a NiTi implant to display these desirable properties (low stiffness, high strength, good ability for bone ingrowth, superelastic or shape-memory effect), the pore size, shape, fraction and connectivity (in particular the size of the fenestrations connecting the pores) need to be optimally designed during processing. Simple and rapid production of NiTi foams is achieved by self-propagating synthesis of NiTi from mixed elemental Ni and Ti powders occurring during sintering [5–7], spark-plasma sintering (SPS) [8] or capsule-free hot isostatic pressing (CF-HIP) [9], performed in such a way that porosity originally

* Corresponding author. Tel.: +1 847 491 3463
E-mail address: ampikaa@gmail.com (A. Bansiddhi).

1742-7061/$ - see front matter © 2008 Acta Materialia Inc. Published by Elsevier Ltd. All rights reserved.
doi:10.1016/j.actbio.2008.06.005

present in the preform or created during the synthesis step is not eliminated. Alternatively, argon can be trapped in NiTi during powder densification and subsequently expanded to form pores [10,11]. The above methods, however, do not allow independent control over pore size, shape and connectivity. This issue can be solved by the use of a temporary space-holder phase during the initial cold compaction of metallic powders into preform which is then removed prior to or during the densification of the elemental or pre-alloyed NiTi powders, e.g., ammonium bicarbonate (NH_4HCO_3) in capsule-free hot isostatic pressing [12] and sodium chloride (NaCl) with a polymeric binder in metal injection molding (MIM) and sintering [13].

Pore collapse and risk of contamination due to binder and space-holder decomposition might still be of concern for the above NiTi foams or other high-melting metal foams densified with temporary space-holders [14–16]. These concerns can be addressed by densifying by HIP an encapsulated mixture of metallic and space-holder powders. Compared with sintering, this method decreases the time for densification and improves the quality of the bond between metal particles, but it requires the use of a permanent (rather than temporary) space-holder which is chemically inert with the metal during the HIP densification. Also, a second step is needed, where the space-holder is removed after densification. This approach was recently demonstrated using sodium fluoride (NaF) as space-holder together with NiTi pre-alloyed powders [17]. The HIP densification temperature (950 °C) was kept below the melting point of NaF (993 °C) to avoid melting the space-holder. However, this relatively low temperature (compared with the 1310 °C melting point of NiTi) led to incomplete densification of the NiTi powders. This problem was solved by a sintering treatment of the NiTi foam after NaF removal, which, however, led to a large reduction in foam porosity. For optimal, single-step densification of NiTi powders in the HIP process, it is thus desirable to exceed the melting point of the space-holder to reach temperatures high enough for rapid diffusion in the metal.

Here, this approach is demonstrated using NaCl, rather than NaF, to densify NiTi powders by HIP densification at 950 and 1065 °C, well above the melting point of NaCl (801 °C). The replacement of NaF by NaCl is desirable for the following reasons: lower cost, greater ease of dissolution in water, reduced corrosive attack of NiTi in aqueous solutions during dissolution [18] and much lower toxicity [19]. The latter property of NaCl is particularly important if the NiTi foams are to be used as biomedical implants, as it is difficult to ascertain with high reliability that all space-holder is removed from the foam.

2. Materials and methods

2.1. Foam fabrication

Pre-alloyed near-equiatomic NiTi powders (nominal composition 48.6 at.% Ni) with 99.9% purity supplied by Special Metals Corp. (NY) were used as a matrix material. The NiTi powders are 44–177 μm in size, are nearly spherical and have smooth surfaces (Fig. 1a). Small satellites are present, indicating that the powders were produce by liquid spraying. The space-holder NaCl powder (99.0% purity from Alfa Aesar, MA) was sieved in the range 62–250 μm, and was cuboidal in shape (Fig. 1b), with a more regular shape than the NaF powders used in previous work [17].

NiTi and NaCl powders were mixed with a volume percentage of 60.0% and 40.0%, respectively, in a twin-shell dry blender for 40 min. The mixture was poured and tapped in two mild steel cans with outer diameter 35 mm and wall thickness 1.6 mm. Each steel can was then evacuated, closed by welding and subjected to HIP densification by UltraClad Corp. (MA) for 4 h under a pressure of 100 MPa at two different temperatures, 950 and 1065 °C (well above the 810 °C melting point of NaCl).

Densified NiTi–NaCl composite samples ($10 \times 10 \times 5\ mm^3$) were cut from the HIP cans using a low-speed diamond saw. Each sample was then suspended in circulating

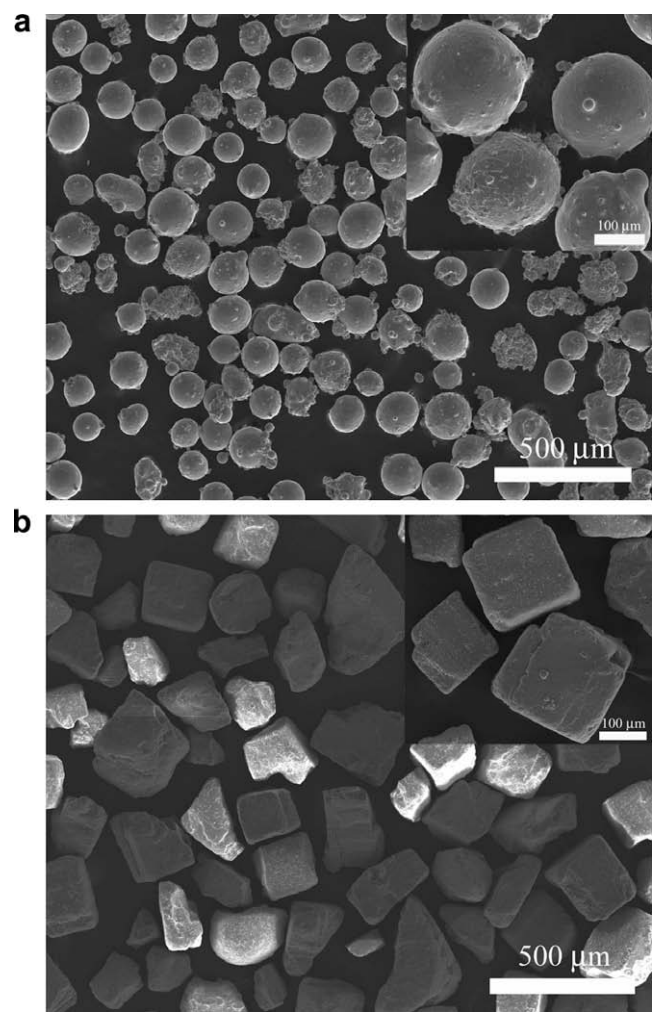

Fig. 1. SEM micrographs of powders used in the HIP process: (a) NiTi and (b) NaCl.

water to dissolve the NaCl, the sample mass being tracked regularly. The dissolution process was terminated when the sample mass was stable and/or decreased to the predicted value equivalent to the mass of starting pure NiTi. Despite the high water solubility of NaCl (35.9 g/100 ml at 25 °C) [19], the leaching process lasted ~2 days. The leached NiTi foams were then cleaned twice in an ultrasonic water bath for 15 min, rinsed with acetone and furnace-dried at 100 °C.

After salt removal, one group of foams was characterized (as described in the next section) in the as-HIP condition; these foams are labeled H1 and H2 for HIP at 950 and 1065 °C, respectively. Another group underwent an additional sintering step at 1250 °C prior to characterization, and these foams are labeled HS1 and HS2 for HIP at 950 and 1065 °C, respectively. The foams were sintered with titanium getters under high vacuum (0.001 Pa gage vacuum) for 4 h, except for an additional HS2 specimen sintered for 24 h (hereafter referred to as HS2′). The sintering heating and cooling rates were 7 K min^{-1}.

2.2. Microstructure characterization

Scanning electron microscopy (SEM) was used to image the cross-sections of 3-mm-thick slices of NiTi foams which were mounted and infiltrated with epoxy resin and polished with 320 μm (sand paper), 9 μm (diamond suspension) and 0.5 μm (alumina) grit. Average pore size was determined by the line-intercept method from SEM images as $1.12L_o/N_{pore}$, where L_o is the line length, and N_{pore} is the number of pores on that line [20]. Closed porosity was measured by helium pycnometry and total porosity by the Archimedes' method in water, after coating the foam surface with a thin layer of grease. Open porosity was calculated by subtracting closed porosity from total porosity. The density of monolithic NiTi used in density calculations was taken as 6.45 g cm^{-3} [21].

The phase transformation behavior was studied on 2–8 mg specimens from foams H1, H2, HS1, HS2 by differential scanning calorimetry (DSC) using a Perkin-Elmer DSC-7 apparatus with a heating and cooling rate of 10 K min^{-1} under nitrogen cover gas. The DSC cycle was performed twice between −60 and 170 °C, and the second cycle was used to determine phase transformation temperatures (from the intersection between the steepest slopes of the peak and the baseline) and the transformation enthalpy (from integration of the peaks) for each foam.

2.3. Mechanical properties measurements

The mechanical behavior of foams H1, H2, HS1 and HS2 was investigated by uniaxial compression experiments at ambient temperature in a screw-driven load frame using a cylindrical cage insuring parallelism. The compressive test samples were cut by electro-discharge machining (EDM) to a $4 \times 4 \times 8$ mm^3 parallelepiped shape. The foams were then lightly polished on 600 grit paper to remove the oxidized surfaces formed during the EDM process, which might affect the mechanical result. The foams were held for 5 min in an oil bath to 160 ± 2 °C (well above the A_f temperature), and then oil-quenched to room temperature prior to the compressive test. The foams were then ultrasonically cleaned in acetone for 20 min, dried and weighed to insure complete removal of oil. The compliance of the testing machine was subtracted from crosshead motion in calculating the foam engineering strain.

A first set of foams (H1 and HS1) was tested at a displacement rate of 0.05 mm min^{-1}, and the tests were ended when load peaked. A second set of foams (H1, HS1, H2 and HS2) was then subjected to a series of load–unload–heat recovery cycles. In the first cycle, the foam was loaded at a constant crosshead displacement rate of 0.05 mm min^{-1} to a maximum strain (ε_{max}) of 1%, unloaded at the same rate, and then heat-treated in oil using the same method described above, to trigger the shape-memory recovery. The foam length was measured by a micrometer with 1 μm accuracy at three points during the test: before loading, after unloading and after heat treatment in oil. The same cycle was then repeated, but with loading to a higher maximum strain (with 1% increments) until signs of a load drop due to foam failure/damage appeared upon loading, or until a maximum strain of 8% was reached.

3. Results

3.1. Microstructure

Figs. 2–4 show that the porous NiTi produced by the present method exhibits an interconnected porous structure, without evidence of reaction between the molten NaCl and solid NiTi. Both the blocky shape and the ~100 μm size of the pores are similar to those of the initial NaCl powders (Fig. 1b). Foams H1 and HS1 have a total porosity of 36 ± 0.1% (31 ± 0.1% open porosity) and 35 ± 0.1% (34 ± 0.2% open porosity), with pore sizes 167 ± 13 μm and 151 ± 23 μm, respectively. Although pore size and fraction before and after sintering are almost the same, the pore walls of foam HS1 after sintering shows significantly higher levels of densification than those of foam H1, as visible by comparing Fig. 2b and d, resulting in a smoother surface of the large pores, and a reduction of the small pores within the walls.

The total porosity of the foams HIP-densified at the higher temperature (32 ± 0.1% for H2 and 32 ± 0.5% for HS2) is lower by ~3–4% than for the foams H1 and HS1 densified at the lower temperature, but their open porosity remains high (30 ± 0.1% for H2 and 28 ± 0.7% for HS2). Pore sizes for foams H2 (156 ± 22 μm) and HS2 (130 ± 16 μm) are unchanged compared with foams H1 and HS1, within the large experimental error. Except for the small decrease in open porosity, there is no clear difference between foams H2 and HS2, as evident from comparing Fig. 3b and d, indicating that the sintering step had very little effect on the foam microstructure, including the

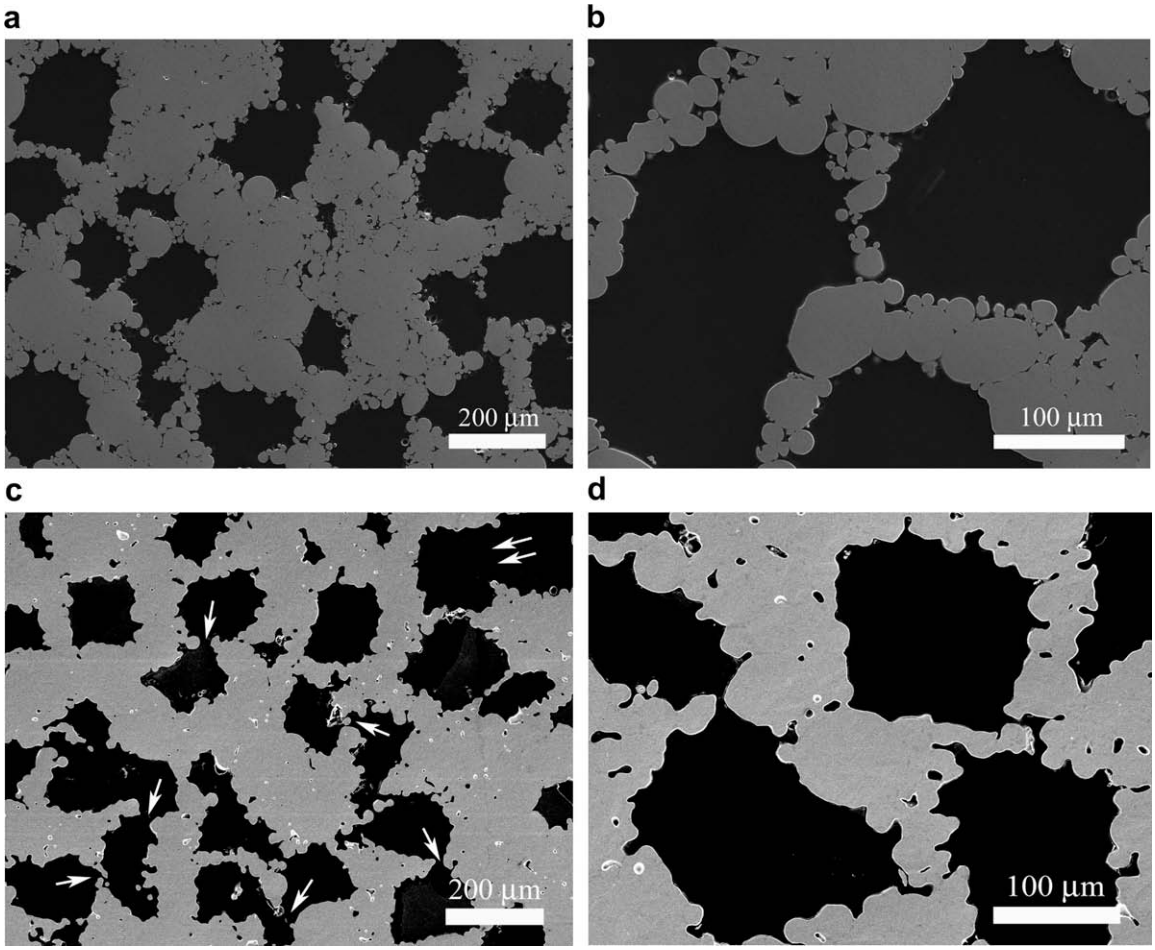

Fig. 2. SEM micrographs of foam cross-sections with resin-filled pores: (a and b) foam H1 (HIP-densified at 950 °C, $P = 36\%$); (c and d) foam HS1 (with additional 1250 °C sintering, $P = 35\%$).

surface roughness of the large pores.Densification of the pore walls (i.e., removal of the small pores within the walls and smoothing of the wall surface) is improved, however, by extending the sintering time at 1250 °C from 4 to 24 h, as demonstrated in Fig. 4 for foam HS2′. The large pores show much smoother surface compared with foam HS2 (Fig. 3d), and most of the small pores within the metallic walls have disappeared. The total porosity is slightly reduced (from $32 \pm 0.5\%$ for HS2 to $31 \pm 0.1\%$ for HS2′) but the open porosity is constant at 28%. This indicates that the closed porosity (expected to be mostly the small pores within the walls) has been reduced from 4% for foam HS2 to 3% for foam HS2′.

3.2. Phase transformation behavior

Fig. 5 displays DSC curves for all four foams upon heating and cooling which, for clarity, are shifted along the y-axis. The presence of a single peak upon cooling indicates the absence of any intermediate phase between the high-temperature austenitic phase and the low-temperature martensitic phase. The transformation enthalpy and temperatures determined from these curves are listed in Table 1: they are similar for all foams and are typical of bulk NiTi (enthalpy of 24.3 J g^{-1} [21]). However, foam H1 has somewhat lower transformation temperatures (by 5–6 °C) than foam H2, which was densified at a higher temperature, and the DSC curves of the two foams subjected to the additional sintering step (HS1 and HS2) are broadened by 10–15 °C compared with foams H1 and H2. With M_f values of 47–59 °C, all foams are martensitic at room and body temperature, and are thus expected to show the shape-memory effect at these temperatures, as discussed in the following section.

3.3. Mechanical and shape-memory properties

Fig. 6 shows compressive stress–strain curves for foams H1 and HS1 for experiments performed under monotonic loading conditions. Foam H1 reaches a stress of ~200 MPa and a strain ~6% before the stress drops. By contrast, foam HS1 can withstand compressive stresses of 1060 MPa after being deformed to ~42% strain. This illustrates the strong improvement in wall strength achieved by sintering, despite nearly unchanged size, shape and fraction of the large pores.

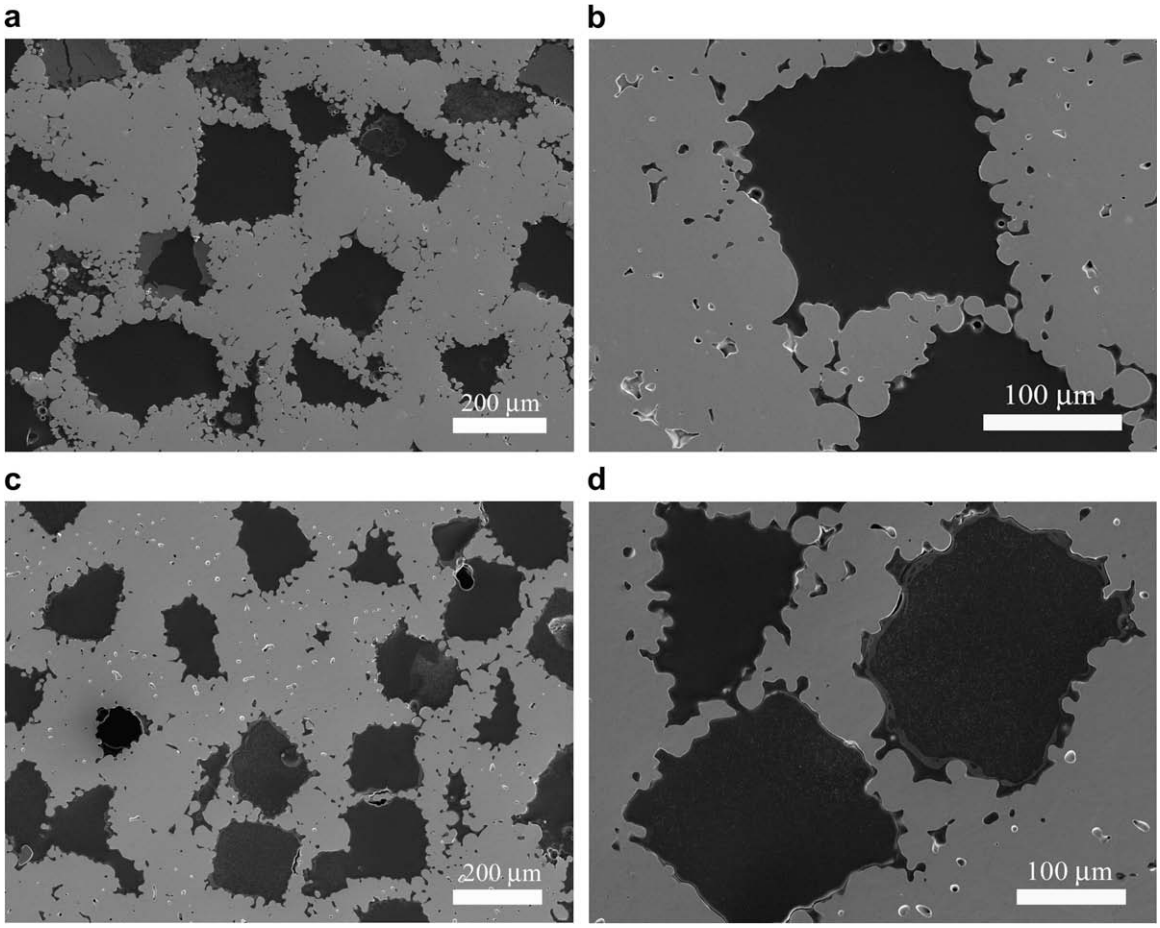

Fig. 3. SEM micrographs of foam cross-sections with resin-filled pores: (a and b) foam H2 (HIP-densified at 1065 °C, $P = 32\%$); (c and d) foam HS2 (with additional 1250 °C sintering, $P = 32\%$).

The load–unload–heat recovery cycles of foam H1 and HS1 are shown in Fig. 7a and b, with curves shifted along the x-axis for clarity. Foam H1 underwent five cycles (up to 5% maximum strain), before damage in the sixth cycle at 6% strain led to a stress drop. After sintering, the foam HS1 underwent eight compressive tests (up to 8% maximum strain at 400 MPa) without failure. The cyclic behav-

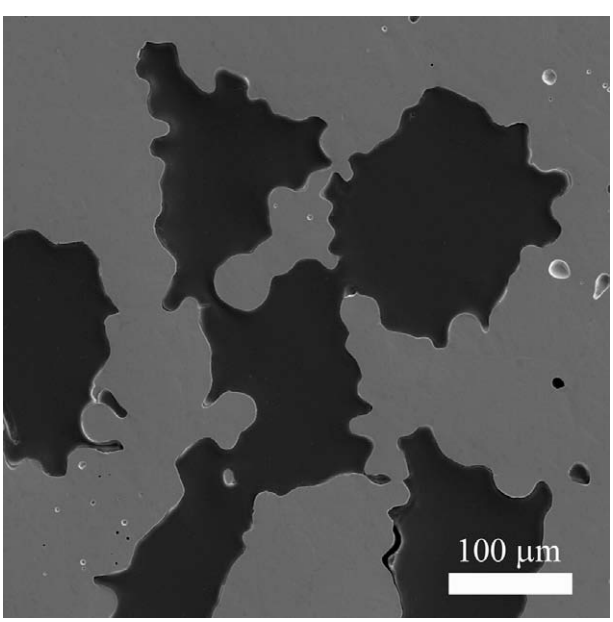

Fig. 4. SEM micrograph of cross-section of foam HS2′ (same process as HS2, except for longer sintering duration at 1250 °C, $P = 32\%$).

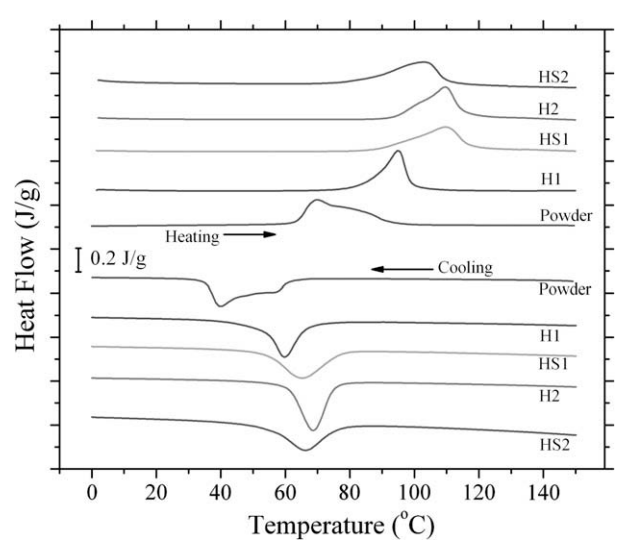

Fig. 5. DSC curves of NiTi powder and foams H1, H2, HS1 and HS2.

Table 1
Transformation temperatures and enthalpies for as-received NiTi powders and foams H and HS

	Powder	Foam H1	Foam HS1	Foam H2	Foam HS2
Process	As-received	HIP (950 °C)	HIP (950 °C) + sinter (1250 °C)	HIP (1065 °C)	HIP (1065 °C) + sinter (1250 °C)
Heating					
A_s (°C)	63	85	81	91	77
A_f (°C)	93	98	106	104	103
Enthalpy (J g^{-1})	24	22	24	25	22
Cooling					
M_s (°C)	61	65	72	71	68
M_f (°C)	35	54	51	59	47
Enthalpy (J g^{-1})	24	22	23	24	22

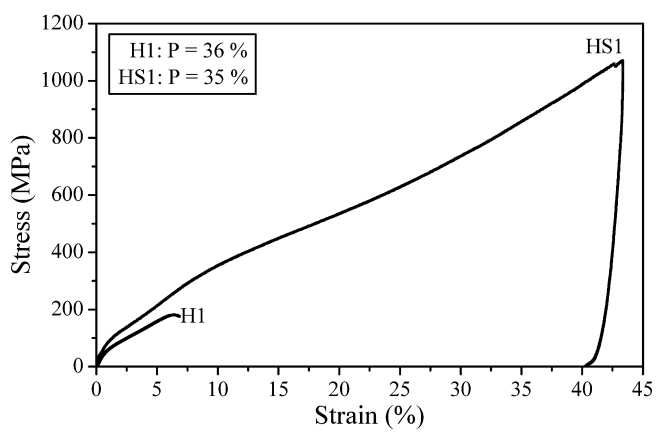

Fig. 6. Compressive stress–strain curves for foams H1 and HS1 upon monotonic loading until onset of stress drop.

ior of both foams (Fig. 7a and b) is in agreement with the monotonic curves of Fig. 6. Finally, the cyclic compressive behavior of foam H2, which was HIP-densified at the higher temperature, is shown in Fig. 7c and is nearly identical to that of foam HS1 (Fig. 7b). The eight curves for foam HS2 (deformed in 1% increments to a maximum strain of 8%) are not shown, as they are similar to those of foams HS1 and H2, as expected from the similar foam microstructures.

For each load–unload–heat recovery cycle, loading stiffness (E_{load}), unloading stiffness (E_{unload}), unloading strain recovery (ε_{unl}), thermal strain recovery (ε_{rec}), and plastic strain after recovery (ε_{pl}) were determined from the engineering stress–strain curves, as illustrated in Fig. 7a, in a manner similar to a previous study of NiTi foams with NaF space-holders [17]. The loading stiffness was determined from the slope of a best linear fit of the loading curve, ignoring data below 10 MPa to avoid sample settling effects. The same approach was used to find the unloading stiffness, but only data between 10 MPa and $\sigma_{max}-10$ MPa were taken into account, to avoid the steep stress drop at the beginning of unloading due to machine mechanical hysteresis. The unloading strain recovery was calculated from the length change on unloading from maximum to zero stress. Similarly, the thermal strain recovery was found from the difference in sample length before and after the heat-recovery treatment. Finally, the plastic strain was calculated from the difference in sample length before and after the full thermo-mechanical loop.

Shape-memory recovery was observed in all cycles of all foams and represents a large fraction (59–100%) of the plastic strain after unloading. Generally, the fraction of strain recovered by shape-memory is constant with increasing maximum strain, as illustrated for foam H2 in Fig. 8. Also shown in this figure are the unload and plastic strains, both of which increase linearly with the maximum strain.

Finally, Fig. 9 shows the stiffness on loading and unloading for all four foams. It is apparent, as expected from the shape of the stress–strain curves, that loading stiffness is much lower (by a factor of 2–5) than the unloading stiffness. Also, the loading stiffness remains near constant with increasing maximum strain, while the unloading stiffness increases.

4. Discussion

4.1. Process

The principal motivation for using molten NaCl as space-holder is to access high temperatures during the HIP densification to improve the metal powder densification kinetics, without the use of a high-melting space-holder such as NaF ($T_m = 993$ °C) for NiTi foams [17] or BaF_2 and SrF_2 ($T_m = 1368$ and 1473 °C) for Zr-based foams [22]. Compared with these fluorides, NaCl is inexpensive, has much higher solubility in water (thus facilitating dissolution), does not form fluoride ions during dissolution (which can pit the foam and have high toxicity, which is problematic if the foam is to be used as a biomedical implant), and can be easily synthesized in various powder shapes [23], allowing modification of pore shape, connectivity and surface roughness.

In the past, NaCl has been used as a space-holder for aluminum foams made by liquid metal infiltration [24] or by sintering [25] and spark plasma sintering [26], but always below its melting point. NaCl space-holders were also used in a MIM process for making porous NiTi [13] but were removed before the sintering process, which took place at a temperature higher than its melting point. Thus,

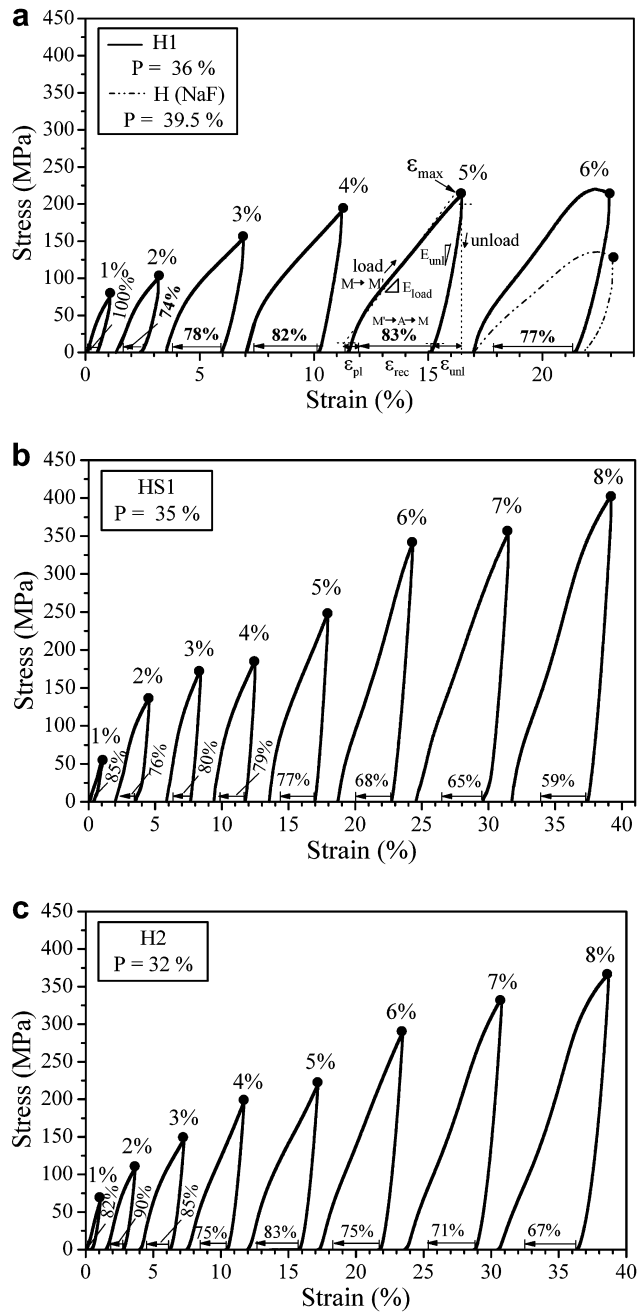

Fig. 7. Series of compressive stress–strain curves (load–unload–recovery cycles for increasing maximum strains) for: (a) foam H1, including the last stress–strain curve of foam H produced with NaF space-holders [17]; (b) foam HS1; (c) foam H2. Curves are shifted along the x-axis for clarity. Arrows along the x-axis for each curve represent the thermally recovered shape-memory strain. The stress at which the foam is unloaded is marked with a dot. Parameters used in evaluation method for loading and unloading stiffnesses, and for the unloading, shape-memory and plastic strains are illustrated, together with the phases expected (A, austenite; M, martensite; M′, de-twinned martensite), in the stress–strain curve to 5% maximum strain in (a).

to the authors' knowledge, this is the first time that metallic powders have been densified in the presence of a molten (rather than solid) space-holder to produce a metallic foam.

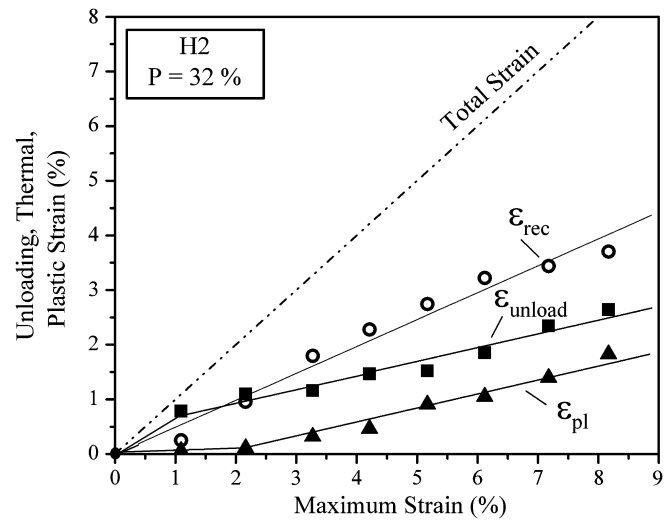

Fig. 8. Unloading, shape-memory, and plastic strain as a function of maximum compressive strain for foam H2.

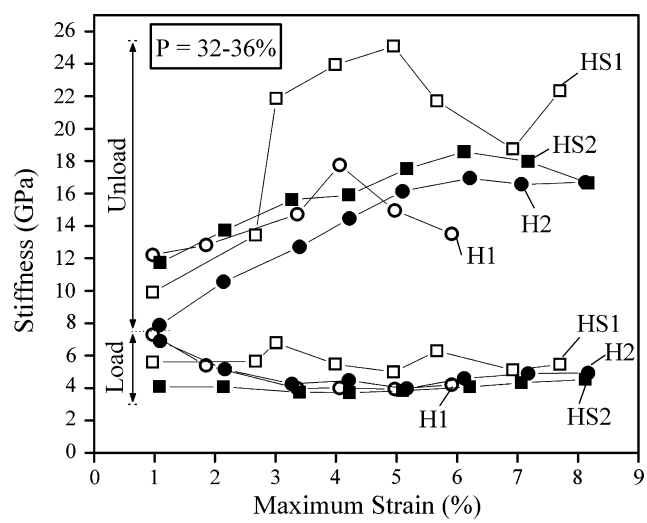

Fig. 9. Loading and unloading stiffness as a function of maximum compressive strain for all foams.

Comparison of microstructure and properties for the NiTi foams H1 and H2 shows that the increase in densification temperature from 950 to 1065 °C is accompanied by a notable improvement in metal powder densification and mechanical properties. The first HIP temperature of 950 °C was chosen to compare the H1 foams with those obtained at the same HIP temperature using solid NaF space-holder in a previous work [17]. The second HIP temperature of 1065 °C was selected because it is below the Fe–Ti eutectic temperature at 1085 °C, which may have led to liquid formation by reaction of NiTi with the HIP steel can.

The main challenges associated with the use of a molten space-holder during metal powder densification are as follows. First, the molten space-holder may react chemically with the metal. However, the free energies of formation of solid and liquid NaCl are much lower than those of

$NiCl_2$ and $TiCl_4$ [27], and there appear to be no mixed halides containing both Na and Ni or Ti. Second, the molten space-holder may dissolve the metal. For the NiTi–NaCl combination, this is unlikely to occur, as synthesis of equiatomic NiTi powders was reported to be possible in molten NaCl + KCl salts at 680–800 °C, starting from elemental Ni and Ti powder, and the resulting NiTi particles exhibited a reversible martensitic transformation, indicating high purity [28]. Third, the molten space-holder may wet the metal powders thus preventing their densification by creating a thin layer of liquid between them. This did not occur in the present case, indicating that molten NaCl poorly wets NiTi and/or that the NiTi powders were sufficiently densified during the HIP temperature ramp prior to NaCl melting.

4.2. Microstructure

The rectangular cross-sectional shape of the pores of HIP-densified foams H1 and H2 (Figs. 2a,b and 3a,b) indicates that the solid NaCl particle shape (Fig. 1b) is well replicated. Partially densified, spherical NiTi particles are clearly visible in the walls of foam H1 (Fig. 2a and b), so that the large pores have a very rough surface, and the walls contain numerous small pores which seem to be often closed. By contrast, the degree of densification between spherical NiTi powders is much improved in foam H2 densified at higher temperature, or in foam HS1 sintered after the low-temperature HIP step. Accordingly, the surface roughness of the large pores and the porosity within the metallic walls are reduced, translating to stronger walls and improved foam strength.

The rectangular shape of the pores indicates that NiTi powders densified into a rigid matrix, before the NaCl melted, during the temperature ramp of the HIP process which occurred under pressure. At the HIP pressure of 100 MPa, the melting point of NaCl is ~20–30 °C above its 801 °C value at 1 atm [29]. This modest increase in the melting point of NaCl should have little impact on the process. Under hydrostatic pressure conditions, the driving force for spheroidization of liquid-filled pores is the reduction in interfacial energy. The lack of pore spheroidization may be indicative of a relatively low interfacial energy, and/or a relatively low surface diffusion coefficient, expected given the moderate value of the homologous temperature. In fact, sintering in vacuum at markedly higher temperature (1250 °C) for a long time (24 h) did not affect the rectangular shape of the large pores but merely smoothed the pore edges and densified the small porosity within the NiTi walls. The lack of trapped NaCl in closed porosity also indicates that NiTi densification was sufficient prior to NaCl melting to prevent liquid NaCl from infiltrating the NiTi preform. It is unknown whether molten NaCl wets NiTi, but the HIP pressure was most probably high enough to induce pressure infiltration if much open porosity was available in the NiTi preform. Thus, it appears that NiTi pre-densification was sufficient for the liquid NaCl to remain within the blocky pores and prevent their collapse from the HIP pressure, but without much liquid infiltrating the small spaces remaining between the prior NiTi powders. Also, most of the pores in the H1 foam are more regular in shape than those in previous foams made with solid NaF space-holder by HIP at the same temperature (950 °C) [17]; this is due to the more uniform shape of the NaCl particles. Furthermore, fewer small pores were observed in the present foams owing to better sieving of NaCl, which may explain why the present foams showed much less densification after 24 h sintering compared with equivalent foams made with NaF space-holders with a larger fraction of small particles [17].

The porosity of the foams after the HIP process (32–35%) is lower than the expected value of 40% based on the NaCl volume fraction initially present in the mixed powders. The cause might be a heterogeneous distribution of NaCl particles in the initial powder mixture during filling into the HIP can, or a small relocation of molten NaCl to walls of the HIP cans through connecting pore channels, as it is squeezed by the high HIP pressure. Closed porosity of ~2–3% is present as small pores (~10 μm in size), owing to incomplete densification between NiTi powders and possibly trapped NaCl vapor which prevents full densification. This amount is small compared with the microporosity observed (from micrographs) in other studies that rely only on pressureless sintering with NaCl space-holders [13] or on the use of gas-decomposable space-holders [12].

The average pore size is in the range 130–170 μm for all foams, which is above the minimum value at which bone ingrowth is possible (~50 μm) [30]. The pore size was determined by the size of NaCl particles (62–250 μm), with some large pores resulting from their agglomeration. This range of particles was selected to avoid excessively large pores (>500 μm) resulting from contact between adjacent NaCl particles, which may not be optimal for bone ingrowth and may weaken implants with small cross-sections. In general, this indicates that pore characteristics (pore fraction, shape and size) can be tailored in the NiTi foams by the fraction, shape and size of the NaCl used as space-holder.

After sintering at 1250 °C for 4 h (foams HS1 and HS2 in Figs. 2c,d and 3c,d), the pores remain rectangular in shape, indicating that diffusivity (both surface and bulk) is insufficient to alter these large pores significantly. The pore surfaces smoothes out only incompletely, again indicating that the diffusivity is low. However, foam HS2′ sintered for 24 h shows clear further smoothing of the pore surfaces (Fig. 4). The sintering temperature of 1250 °C cannot be raised further, given that it is close to the melting temperature of NiTi (1310 °C) and that the solidus of NiTi decreases rapidly, even with small deviations from stoichiometry [21]. Since increasing sintering times significantly beyond 24 h is costly and may lead to contamination from residual gases in the vacuum furnace, increasing the HIP time, temperature and pressure are more practical

approaches to improving the densification of the NiTi powders further. Indeed, raising the HIP temperature from 950 to 1065 °C seems to be as effective as adding a sintering step at 1250 °C, when comparing the microstructure and mechanical properties of foams HS1 and H2. Use of elemental Ni and Ti powders during HIP densification with molten NaCl space-holders may also be an alternative option.

The benefits of HIP densification on powder consolidation are likely to be more visible at higher porosity, which is desirable for implant applications [31], where thinner NiTi walls need to be densified while maintaining the pore structure without pore collapse. A simple sintering approach with transient space-holder may be problematic for such foams, as some difficulties were noted [13] when producing NiTi with 70% porosity using pre-alloyed NiTi powder and NaCl space-holder. Moreover, the same method could be used to produce Ni-rich superelastic NiTi foams, instead of the foams with shape-memory properties demonstrated here, which would provide larger recovery strain and even lower stiffnesses suitable for reducing stress-shielding effect. The near-net shape manufacturing of implants with complex shapes by the present HIP consolidation may be difficult, so this method may be more appropriate for the creation of rough-shape objects that will necessitate a final machining step.

No NaCl residues were observed in cross-sections. This concurs with chemical analysis results (performed Luvak Inc., MA), which detected 0.041 and 0.065 wt.% sodium and chlorine in a 2 g sample of foam HS2. This corresponds to 2 mg of residual NaCl, which is well below the NaCl concentration in human blood, and is so small that it is unlikely that it originates from residual NaCl within the 2–3 vol.% of closed pores. Residual NaCl in open pores is not expected, especially after vacuum sintering, when the foams were subjected to a dynamic vacuum of ~0.001 Pa much lower than the vapor pressure of liquid NaCl (estimated as 18 kPa at 1250 °C by extrapolating available data [32]), so that NaCl is expected to near completely evaporate under these conditions. This opens the possibility of simplifying the NaCl removal process by replacing the lengthy water dissolution step by a vacuum evaporation step, which may further be carried out at a temperature where sintering of the foam walls can also take place.

Porous NiTi with 50% interconnected pores produced by the MIM process with NaCl space-holder removed by water dissolution and followed by sintering at 1250 °C was performed in conjunction with a HMSC cell culture test. Adhesion and proliferation of the cells on the porous NiTi was found after 8 days, indicating that any residual NaCl after the sintering process, similar to the one used here, did not affect the *in vivo* performance of porous NiTi [13].

One concern in the microstructure of the present foams is that the fenestrations connecting adjacent pores might be much smaller than the pore size, thus restricting the ingrowth of bone tissue for foams used as implants, unlike the larger fenestrations in the porous NiTi (42% porosity) produced by capsule-free hot isostatic pressing [12]. Narrow fenestrations are indicated by arrows in Fig. 2c, but these two-dimensional sections may not represent the true width of the fenestrations (indeed, one large fenestration is marked with a double arrow in Fig. 2c). Since the pore connectivity directly reflects the contact area of the space-holder powders, changes in NaCl powder volume fraction, shape and size (compared with NiTi powder size) may lead to more open fenestrations. Alternatively, widening of the fenestrations by chemical dissolution may also be possible.

4.3. Phase transformation behavior

Table 1 shows that the transformation temperatures of the NiTi foams are affected little by the foaming process (transformation temperatures for the as-received powders are lower most probably because of their rapid cooling). The use of pre-alloyed NiTi powders, rather than elemental Ni and Ti powders, insures that no significant deviation from stoichiometry occurs during processing, e.g., through formation of other Ni–Ti phases. Furthermore, the low content of impurities in the powders (0.1 wt.% oxygen and 0.003 wt.% carbon, as measured by Luvak Inc., MA) insures that no titanium oxides or carbides are present, which may change the Ni/Ti ratio and thus affect the transformation temperatures and mechanical properties [33]. Finally, the closed steel cans used to encapsulate the powders prevented increases in impurity levels during HIP densification, as did the use of high vacuum during the sintering step. Also, the transformation enthalpy remains constant for all foams, and is close to the literature value for bulk NiTi (24.3 J g^{-1}) [21]. This confirms that no signification reaction with molten NaCl or oxidation took place during the HIP densification, water dissolution and optional sintering steps. The broadening of the DSC curve after sintering may be the result of different cooling rates or possibly slight oxidation leading to a slight enrichment in Ni in the regions near the surface. Finally, the transformation temperatures for all NiTi foams are above body temperature, so these foams are martensitic at both body and room temperature (where mechanical tests were performed), and they are expected to deform by de-twinning of the martensitic grains and to recover by thermal transformation through the shape-memory effect, as discussed in the next section.

4.4. Mechanical behavior

4.4.1. Maximum strength

The maximum strength of foam H1 with 36% porosity (200 MPa at strain 5.3%, Fig. 6) is close to those of an austenitic NiTi foam (245 MPa) with 42% porosity produced by gas expansion [10] and austenitic NiTi foams (180 MPa) with 30–40% porosity produced by sintering of elemental powders [34]. This is twice the strength at

the same strain of a martensitic NiTi foam with 50% porosity produced with NaCl space-holder by warm pressing and sintering [13]. However, foam H1 starts to fail at ~6% strain, which suggests a weaker porous structure. A martensitic NiTi foam produced with NaF as space-holder shows the same tendency to early failure [17], but with a lower failure strength (135 MPa), explainable by higher porosities (39.5%) both between the walls (due to the space-holder) and within the walls (due to incomplete densification). This is illustrated in Fig. 7a, where the last stress–strain curve (at 6% maximum strain) of a NiTi foam HIP-densified with NaF space-holder [17] is superimposed on that of foam H1 produced here with NaCl.

After the additional sintering step, foam HS1 has a much higher maximum strength (>1000 MPa at >42% strain) than foam H1, as expected from the higher level of densification of the walls (Fig. 2a and b vs Fig. 2c and d). Foam H2 (HIP-densified at the higher temperature) has, however, a maximum strength comparable with that of foam HS1 (HIP and sintered), as expected from their similar levels of wall densification (Fig. 2c and d vs Fig. 3a and b). Additional sintering of foam H2 does not improve its strength, in agreement with the lack of improvement in wall densification. Only after extensive sintering (24 h) are the walls more densified (foam HS2′, Fig. 4), but this is a lengthy procedure that increases the risks of contamination or oxidation. A simpler approach to improving foam strength and wall densification further is to conduct the HIP densification for a longer time (beyond the time of 4 h used here) and/or a higher temperature (beyond the temperature of 1065 °C used here), which may necessitate the use of a diffusion barrier between the steel can and the powders.

4.4.2. Stiffness

The stress–strain curves of foam H1 (Fig. 7a) show an inflection at stresses of 50–80 MPa, indicative of yield, which is expected to occur by de-twinning, given the martensitic structure of the NiTi. Beyond yield, however, the strain-hardening is high, so that the overall shape of the curve on loading is almost linear. This near linearity is even more marked for foams HS1 and H2 (Fig. 7b and c), which may be due to the onset of de-twinning at very low stresses. The average stiffness on loading, which is determined here as a linear best fit of data between 10 MPa to maximum stress, then represents a combination of elastic and de-twinning deformation. On unloading, however, deformation is completely elastic (assuming no reverse de-twinning), and the stiffness is then closer to a true Young's modulus. As expected, the unloading stiffness is much higher than the average loading stiffness, as shown in Fig. 9 for all the foams studied here. The loading stiffness seems to be near independent of the maximum strain achieved, except possibly at the lowest strain of 1%, but this might be due to measurement errors at low stress. By contrast, the unloading stiffness increases significantly with increasing maximum strain, which probably reflects densification of porosity between and within the pore walls.

The unloading stiffness of foams H1, H2 and HS2 (10–18 GPa) is within the stiffness range of cortical bone (12–17 GPa), making these foams attractive for bone implant application. For comparison, a NiTi foam produced with NaF space-holders with 39.5% porosity exhibited a similarly low unloading stiffnesses (12–16 GPa), but with a much lower failure stress of 135 MPa [17]. The unloading stiffness E of foams H1, H2 and HS2 are lower than values predicted by Gibson and Ashby [3], $E = (1–P)^2 E_{NiTi} = 26–29$ GPa, using a porosity $P = 35\%$ and Young's modulus of monolithic NiTi $E_{NiTi} = 61–69$ GPa [2]. This may be the result of slight reverse de-twinning during unloading. Only foam HS1, with unloading stiffnesses of 18–25 GPa beyond 3% maximum strain, comes close to these theoretical values (Fig. 9). The reason for this increased stiffness is unknown.

4.4.3. Strain recovery

As illustrated in Fig. 7a, the maximum strain reached prior to mechanical unloading is the sum of three strains: the elastic unloading strain (ε_{unl}) and the shape-memory strain (ε_{rec}) which are recovered on unloading and during the thermal excursion, and the residual plastic strain (ε_{pl}). Fig. 8 shows these three strains as a function of the maximum strain reached for each of the eight loops to which foam H2 was subjected (Fig. 7c). It is apparent from Fig. 8 that all three strains increase near linearly with the maximum strain, and that the shape-memory recovery strain has the largest magnitude, followed by the elastic unloading strain and the plastic strain. For example, at the maximum strain of 8%, these strains are ~4%, 2.5% and 1.5%, respectively. These three strains are nearly the same, at a given maximum strain up to 6%, as those measured on a NiTi foam produced by HIP densification of NaF space-holders with somewhat higher porosity (39.5% vs 32.2%) [17]. This suggests that the shape recovery behavior of these replicated NiTi foams is not affected by the pore shape or sizes (which were somewhat different between these foams). Also, the same amount of unloading strain at the same maximum strain was reported in a martensitic NiTi foam (with a higher porosity of 50%) produced with NaCl space-holder by hot pressing and sintering [13].

5. Conclusions

This research demonstrates a new foam replication process, where metallic powders (NiTi) are densified in the presence of a permanent space-holder (NaCl) by hot-isostatic pressing at temperatures (950 or 1065 °C) above the melting point of the space-holder (801 °C), so as to improve densification of the metal powders. Despite the melting of the space-holder during the process, there was no sign of reaction with the NiTi powders. After NaCl dissolution, the NiTi foams consisted of 32–36% interconnected porosity with pores size 70–400 μm. The pores

maintained the angular shape of the original NaCl particles, indicating that substantial NiTi densification occurred prior to NaCl melting. Thus, NaCl can be used as a space-holder for NiTi (and other metallic) foams, despite its low melting point, with the following advantages compared with higher-melting permanent space-holders such as fluorides or oxides used to date without melting: lower cost, greater flexibility in powder shape, faster dissolution in water, reduced corrosive attack of metal during dissolution, and lower toxicity. The latter point is particularly important if space-holder residues remain in foams used as bone implants.

The compressive stress–strain curve of the foams are characterized by: (i) a near-linear loading branch, with an average stiffness of 4–6 GPa due to a combination of elastic and de-twinning deformations; (ii) a high failure stress in excess of 1000 MPa (except for the foam HIP-densified at 950 °C with insufficiently densified NiTi walls); (iii) a near-linear unloading branch, with a higher stiffness of 10–25 GPa due to elastic recovery strains; (iv) a shape-memory recovery strain increasing linearly with the maximum applied strain, and reaching a value of ~4% for an applied strain of 8%.

These foams are excellent candidates for bone implant applications, as they exhibit a unique combination of attributes: (i) simple processing route; (ii) desirable mechanical properties (low effective stiffness to alleviate stress shielding; high strength and ductility to prevent failure; shape-memory capability useful to deploy the foam); (iii) biocompatibility (for NiTi) and very low toxicity (for NaCl, if traces remain in the foam); and (iv) large pores fully open to the surface (for bone ingrowth).

Acknowledgments

This research was supported by the US National Science Foundation (Grant DMR-0505772). A.B. also gratefully acknowledges the support, through the Royal Thai Government Scholarship, of the Ministry of Science (Thailand). Useful discussions with Prof. S.I. Stupp (Northwestern University) are acknowledged.

References

[1] Ryan G, Pandit A, Apatsidis DP. Fabrication methods of porous metals for use in orthopaedic applications. Biomaterials 2006;27:2651–70.
[2] Dunand DC, Mari D, Bourke MAM, Roberts JA. NiTi and NiTi–TiC composites IV: neutron diffraction study of twinning and shape-memory recovery. Metall Mater Trans A Phys Metall Mater Sci 1996;27:2820–36.
[3] Gibson LJ, Ashby MF. Cellular solids. Cambridge: Cambridge University Press; 1997.
[4] Yahai L, editor. Shape memory implants. Berlin, New York: Springer Verlag; 2000. p. 349.
[5] Jiang HC, Rong LJ. Ways to lower transformation temperatures of porous NiTi shape memory alloy fabricated by self-propagating high-temperature synthesis. Mater Sci Eng A Struct Mater Prop Microst Proc 2006;438:883–6.
[6] Chu CL, Chung JCY, Chu PK. Effects of heat treatment on characteristics of porous Ni-rich NiTiSMA prepared by SHS technique. Trans Nonferrous Met Soc China 2006;16:49–53.
[7] Biswas A. Porous NiTi by thermal explosion mode of SHS: processing, mechanism and generation of single phase microstructure. Acta Mater 2005;53:1415–25.
[8] Zhao Y, Taya M, Kang YS, Kawasaki A. Compression behavior of porous NiTi shape memory alloy. Acta Mater 2005;53:337–43.
[9] Yuan B, Zhang XP, Chung CY, Zhu M. The effect of porosity on phase transformation behavior of porous Ti-50 .8 at. % Ni shape memory alloys prepared by capsule-free hot isostatic pressing. Mater Sci Eng A Struct Mater Prop Microst Proc 2006;438:585–8.
[10] Lagoudas DC, Vandygriff EL. Processing and characterization of NiTi porous SMA by elevated pressure sintering. J Intell Mater Syst and Struct 2002;13:837–50.
[11] Greiner C, Oppenheimer SM, Dunand DC. High strength, low stiffness, porous NiTi with superelastic properties. Acta Biomater 2005;1:705–16.
[12] Zhang YP, Yuan B, Zeng MQ, Chung CY, Zhang XP. High porosity and large pore size shape memory alloys fabricated by using pore-forming agent (NH_4 HCO_3) and capsule-free hot isostatic pressing. J Mater Proc Tech 2007;192:439–42.
[13] Kohl M, Bram M, Buchkremer P, Stover D, Habijan T, Koller M. Production of highly porous near-net-shape NiTi components for biomedical applications. In: Lefebvre P, Banhart J, Dunand DC, editors. Proceedings of the fifth international conference on porous metlas and metallic foams, DEStech Publications, Inc.; 2008. p. 295–8.
[14] Bram M, Stiller C, Buchkremer HP, Stover D, Baur H. High-porosity titanium, stainless steel, and superalloy parts. Adv Eng Mater 2000;2:196–9.
[15] Laptev A, Bram M, Buchkremer HP, Stover D. Study of production route for titanium parts combining very high porosity and complex shape. Powder Metall 2004;47:85–92.
[16] Li M, Liu Y, Ye JW, Zhang LF, Li J, Tu MJ. Process and compressive properties of porous nickel materials. Powder Metall 2006;49:114–7.
[17] Bansiddhi A, Dunand D. Shape-memory NiTi foams produced by solid-state replication with NaF. Intermetallics 2007;15:1612–22.
[18] Li XJ, Wang JQ, Han EH, Ke W. Influence of fluoride and chloride on corrosion behavior of NiTi orthodontic wires. Acta Biomater 2007;3:807–15.
[19] Patnaik P. Handbook of inorganic chemicals. New York: McGraw-Hill; 2003.
[20] Annual book of ASTM standards: metals test methods and analytical procedures. Metals-mechanical testing; elevated and low-temperature tests; metallography. Philadelphia, PA: ASTM; 2004, pp. 267-292.
[21] Jackson CM, Wagner HJ, Wasilewski RJ, 55-nitinol—the alloy with a memory: its physical metallurgy, properties, and applications. 1972.
[22] Brothers AH, Scheunemann R, DeFouw JD, Dunand DC. Processing and structure of open-celled amorphous metal foams. Scripta Mater 2005;52:335–9.
[23] Gaillard C, Despois U, Mortensen A. Processing of NaCl powders of controlled size and shape for the microstructural tailoring of aluminium foams. Mater Sci Eng A Struct Mater Prop Microst Proc 2004;374:250–62.
[24] Despois JF, Marmottant A, Salvo L, Mortensen A. Influence of the infiltration pressure on the structure and properties of replicated aluminium foams. Mater Sci Eng A Struct Mater Prop Microstr Proc 2007;462:68–75.
[25] Zhao YY, Han FS, Fung T. Optimisation of compaction and liquid-state sintering in sintering and dissolution process for manufacturing Al foams. Mater Sci Eng A Struct Mater Prop Microst Proc 2004;364:117–25.
[26] Hakamada M, Yamada Y, Nomura T, Kusuda H, Chen YQ, Mabuchi M. Effect of sintering temperature on compressive properties of porous aluminum produced by spark plasma sintering. Mater Trans 2005;46:186–8.

[27] Reed TB. Free energy of formation of binary compounds; an atlas of charts for high-temperature chemical calculations. Cambridge, MA, London: MIT Press; 1971.
[28] Zhao JL, Cui LS, Gao WF, Zheng YJ. Synthesis of NiTi particles by chemical reaction in molten salts. Intermetallics 2005;13:301–3.
[29] Akella J, Vaidya SN, Kennedy GC. Melting of sodium chloride at pressures to 65 kbar. Phys Rev 1969;1:1135–40.
[30] Itala AI, Ylanen HO, Ekholm C, Karlsson KH, Aro HT. Pore diameter of more than 100 μm is not requisite for bone ingrowth in rabbits. J Biomed Mater Res 2001;58:679–83.
[31] Imwinkelried T. Mechanical properties of open-pore titanium foam. J Biomed Mater Res Part A 2007;81A:964–70.
[32] Kaufmann DW. Sodium chloride; the production and properties of salt and brine. New York: Reinhold Pub. Corp.; 1960.
[33] Mentz J, Bram M, Buchkremer HP, Stover D. Improvement of mechanical properties of powder metallurgical NiTi shape memory alloys. Adv Eng Mater 2006;8:247–52.
[34] Li BY, Rong LJ, Li YY. Stress–strain behavior of porous Ni–Ti shape memory intermetallics synthesized from powder sintering. Intermetallics 2000;8:643–6.